



Novel orbital drilling and reaming tool for machining holes in carbon fiber–reinforced plastic (CFRP) composite laminates

Linghao Kong¹ · Dong Gao¹ · Yong Lu¹ · Zhipeng Jiang¹

Received: 2 April 2020 / Accepted: 10 August 2020 / Published online: 18 August 2020
© Springer-Verlag London Ltd., part of Springer Nature 2020

Abstract

Carbon fiber–reinforced plastics (CFRPs) have excellent mechanical and physical properties and are widely used to manufacture structural components and skins in aviation and aerospace. Industrial applications impose high requirements on the quality and efficiency of CFRP drilling. However, it is difficult to meet these requirements with conventional methods, such as drilling and orbital drilling. To improve hole processing quality, a novel cutting tool for orbital drilling was proposed in this research. Replacing the end mill in conventional orbital drilling (COD) with this novel cutting tool can enable an orbital drilling and reaming (ODR) machining process, which can suppress defects and reduce the thrust force when machining CFRP composite laminates. The thrust forces, tool wear, cutting temperatures, and hole quality in the ODR process presented in this paper were studied experimentally. The results indicated that machining with the novel ODR tool effectively reduced the thrust force and cutting temperature observed when machining with the general end mill. Moreover, the hole quality and tool life during ODR were exceedingly better than those during COD. The experimental results showed that processing with the novel tool has immense potential to replace existing processing methods for machining holes in CFRP composite laminates.

Keywords Orbital drilling · Thrust force · Delamination · Temperature · CFRP

Nomenclature

d (mm)	Diameter of the milling part
D (mm)	Diameter of the peripheral cutting edges
a_p (mm)	Screw pitch of the helical path
e (mm)	Eccentricity of the helical path
R (mm)	Radius of the arc of the ODR tool
d_{ap} (mm)	Diameter of reaming part at a height of a_p
h (mm)	Height of the reaming part
v_{fa} (mm/rev)	Feed rate in the Z direction
v_{ft} (mm/rev)	Tangential feed rate

$Sp1$	First marked point on the sidewall
$Sp2$	Second marked point on the sidewall
$Sp3$	Third marked point on the sidewall
$Sp4$	Marked point of ambient temperature
$Dt1$ (°C)	Temperature rise between marked point $Sp1$ and the ambient temperature
$Dt2$ (°C)	Temperature rise between marked point $Sp2$ and the ambient temperature
$Dt3$ (°C)	Temperature rise between marked point $Sp3$ and the ambient temperature
F_d	Delamination factor
D_{max} (mm)	Maximum diameter of the damaged zone
D_{nom} (mm)	Hole diameter

✉ Yong Lu
luyong@hit.edu.cn

Linghao Kong
linghao8959@163.com

Dong Gao
gaodong@hit.edu.cn

Zhipeng Jiang
dapeng99@139.com

1 Introduction

Carbon fiber–reinforced plastics (CFRPs) are extensively used in the manufacture of structural components and skins in aviation, aerospace, and defense applications and exhibit excellent mechanical and physical properties, such as light weight, high strength, low thermal contraction, and low thermal expansion [1, 2]. CFRPs are made into skins and load-

¹ School of Mechatronics Engineering, Harbin Institute of Technology, P.O. Box 422, Harbin 150001, People's Republic of China

bearing structures to reduce the weight of aircraft. To connect CFRP components with metal components, a substantial number of rivet and bolt holes must be manufactured in the CFRP parts. For example, Gao et al. [3] reported that an F-16 jet fighter contains 240,000 connecting holes and that there are 3 million connecting holes on a Boeing 747 airplane.

Due to the laminated structure of CFRPs, the interlaminar shear strength and transverse tensile strength of CFRPs are insufficient. Furthermore, the interlayer strength of CFRPs will further decrease under the influence of cutting temperature due to the low glass transition temperature of epoxy resin. This phenomenon will easily cause many machining defects during the drilling process, such as delamination, matrix cracking, fiber pull out, burring, and fuzzing [4, 5]. In particular, delamination is considered to be the most disastrous defect, as this phenomenon results in a significant reduction in stiffness and load carrying capacity of mechanical components. Srinivasan et al. [6] reported that CFRP part rejection due to delamination in the aircraft industry is greater than 60%.

Drilling is one of the most widely used processes in the machining of CFRPs. Bonnet et al. [1] showed that the thrust force is the main reason for the severity of delamination. Drilling can cause severe damage in CFRPs during hole machining. Therefore, the influences of the tool properties and the cutting parameters on the CFRP damage sustained during hole machining have been extensively studied over the past few decades. Twist drills, which are the most widely used tools in drilling, have been extensively studied. Durão et al. [7] compared the effect of the tool geometry and feed rate on machining holes in CFRPs and found that an appropriate selection of tools and machining parameters can effectively reduce the occurrence of delamination. Iliescu et al. [8] compared the influence of coated and uncoated twist drills on the cutting force, the cutting parameters, and the tool wear in the process of CFRP drilling. During the drilling process, the twist drill continuously rotates; however, the cutting speed of the chisel edge is zero. The material below the chisel edge is crushed by squeezing action rather than shearing action [9]. Jain et al. [10] found that the thrust force generated by the chisel edge accounts for approximately 40–60% of the total thrust force of a twist drill. Twist drills cannot meet the high-quality processing requirements of CFRPs [2, 11]. Step drills are also used in CFRP processing to enhance the machining quality. Isbilir et al. [12] compared the machining quality of twist drills and step drills by developing a 3D finite element model for CFRP drilling and showed that the machining performance could be effectively improved by optimizing the step drill geometry. The geometry of the step drill was adjusted to further improve the machining quality. Feito et al. [13] studied the influence of the step drill geometry on machining damage and established a simulation model to predict cutting force and delamination, which can help optimize machining

parameters. Shyha et al. [2] studied the influence of the tool geometry and cutting parameters on the cutting force, torque, delamination factor and tool life when machining with twist drills and step drills. In addition to step drills, some other tools are also used in CFRP machining. Lazar et al. [14] compared the machining process of a double-point angle drill, a tapered drill-reamer, and a twist drill and found that the maximum thrust force was related to the tool geometry and the feed rate, and the spindle speed had nearly no influence. Hocheng et al. [15] theoretically analyzed the processing quality of various tools by calculating the critical thrust forces of a twist drill, a candlestick drill, a core drill, a special core drill, a saw drill, a step drill, and other special drilling tools. To reduce tool wear caused by the cutting temperature, Biermann et al. [16] adjusted the structure of an electroplated diamond core drill to improve the heat dissipation performance and to reduce the processing temperature. In addition to common drilling tools, scholars have also developed new tools for CFRP drilling. Su et al. [17] proposed a novel tool that combined the advantages of a candlestick drill and a double-point angle drill. A novel drill structure based on a tapered drill-reamer that can remove material from a CFRP in the upward direction was proposed by Jia et al. [18]. Butler-Smith et al. [19] pointed out that compared with a traditional core drill, an electroplated diamond core drill can greatly reduce the cutting force and processing temperature in CFRP drilling. Tsao [20] studied the influence of the diameter ratio and machining parameters on the machining effect of step core drills and found that the diameter ratio and feed rate have the most obvious influence on machining performance, and the type of core cutter will affect the maximum thrust force [20]. These types of drills mentioned above are shown in Fig. 1.

The impacts of the drill types (twist drill, candlestick drill, step drill, dagger drill, saw drill, double-point angle drill, 8 facet drill, core drill, and special core drill), tool geometry (diameter, point angle, helix angle, and chisel length), and tool material on delamination have been extensively studied. Drill bits with special structures, such as step drills and saw drills, could achieve superior processing quality with higher processing efficiency than a twist drill. Although the performance of the drilling process has improved with the abovementioned drill bits, sometimes the requirements set by industry, such as high quality, high efficiency, and low cost, are still quite hard to satisfy.

To further improve the quality of hole machining, several hole machining methods have been proposed in recent years, such as orbital drilling, wobble milling [21, 22], vibration-assisted cutting [23], water jet cutting [24], laser cutting [25], and EDM [26]. Orbital drilling (helical milling) is a promising technique for CFRP machining and has already been widely adopted in practice. Pereira et al. [27] summarized the research on orbital drilling, wherein they noted the differences between orbital drilling and conventional drilling

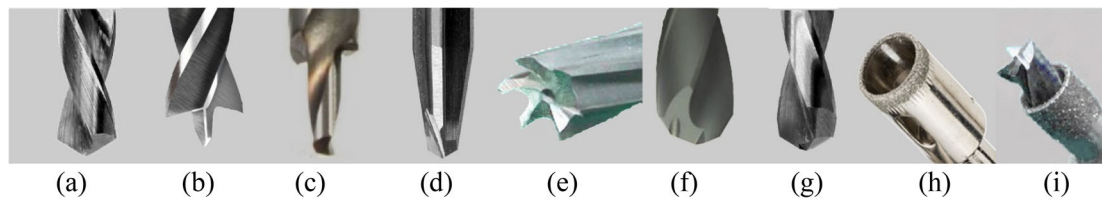


Fig. 1 Images of different drilling tools: **a** twist drill, **b** candlestick drill, **c** step drill, **d** dagger drill, **e** saw drill, **f** double-point angle drill, **g** 8 facet drill, **h** core drill, and **i** special core drill

in terms of kinematics and material removal and outlined the advantages of orbital drilling in processing CFRPs such as the cutting temperature, tool life, and machining performance. Brinksmeier et al. [28] mathematically described the cutting conditions in orbital drilling and showed the computational relationship between the parameters. In this method, an end mill, for which the axis is parallel to the hole to be drilled, rotates around its axis and exhibits planetary motion around the hole axis [29]. Moreover, the end mill moves along a helical path that can be decomposed in the axial direction and tangent direction. Affected by the trajectory, the cutting motion of the orbital drill includes frontal cutting and peripheral cutting. Voss et al. [30] found that in processing CFRPs, orbital drilling is obviously superior to traditional drilling in terms of several factors, including the cutting force, tool life, and processing quality, but the processing time is longer. Ahmad et al. [31] studied the influence of eccentricity, workpiece thickness, and tool surface conditions on the machining quality of orbital drilling with a constant cutting speed and feed rate. Zhou et al. [32] studied the influence of cutting speed and eccentricity on tool life and machining quality in orbital drilling of CFRP/Ti with a dedicated tool. Orbital drilling can effectively improve the quality of machining and supersede traditional drilling. In practice, the orbital drilling process can be accomplished in two ways. One way involves the usage of a multi-axis CNC machining center that generates planetary motions for the tool through interpolation. The other way is accomplished by installing an orbital drilling hole-machining end effector on an NC milling machine or a robot. During the machining process, affected by the eccentricity of planetary motion, the diameter of the drilled hole must be larger than that of the tool. Compared with traditional drilling, orbital drilling has many advantages, the most important of which is that orbital drilling has less thrust force, which can effectively reduce the possibility of delamination. A longer tool life is one of the benefits of orbital drilling since the chips are removed by the helical groove or retained in the radial clearance between the hole and the tool, thereby reducing the friction between the chips and the tool. Another advantage is that the tool cuts the material on the hole wall intermittently, which promotes heat dissipation and improves the processing quality. Therefore, in terms of machining quality, tool life, cutting temperature, and processing efficiency, orbital drilling does have many advantages over conventional drilling.

However, there are still some drawbacks in orbital drilling. In the process of orbital drilling, the cutting edge at the end of the tool keeps cutting constantly, thereby resulting in a high cutting temperature and severe tool wear. The whole end of the tool cuts in and out of the workpiece at approximately the same time, causing a sharp increase and decrease in the thrust force at the hole entrance and exit [29]. More importantly, delamination still occurs frequently. To settle these problems, Ohta et al. [33] developed a tilted planetary drilling system (tilted orbital drilling) based on orbital drilling. The tilted orbital drilling technique is performed by tilting the tool against the workpiece at a small angle during COD [3]. Wang et al. [34] analyzed the machining process and material removal process of orbital drilling and tilted helical milling and pointed out that the machining quality of tilted helical milling is better than that of orbital drilling [34]. However, the stiffness of the machining system is reduced by the tilted orbital drilling technique. Moreover, the processing equipment for this process is more expensive than that used for orbital drilling.

Currently, although scholars have provided various methods to make holes in CFRPs, there still exist substantial demands to meet the needs of industrial applications such as high quality and low cost. Therefore, in this paper, the author proposed a tool to transform orbital drilling to the process of ODR, which can mitigate the generation of defects such as burrs and delamination while reducing the influence of the cutting temperature on the processing effect. The performance of the ODR was compared with the COD process to illustrate the superiority of the tool proposed in this research. The realization of ODR with the dedicated tool is analyzed in Section 2. Section 3 presents the experimental instruments and cutting parameters used in the comparative experiments. Section 4 mainly focuses on the analysis of the experimental results, including thrust force, tool wear, cutting temperature, and hole-exit quality. In the last section, the conclusions are reached.

2 Process of ODR

2.1 Realization of ODR

Research and practical experience indicate that step drills and orbital drilling are very suitable for reducing the damage sustained while machining CFRPs. To reduce the defects at

the exit and improve the machining performance, a novel machining process combining the advantages of step drills and orbital drills is proposed, as shown in Fig. 2. The ODR process is performed by replacing the end mill in COD with a dedicated tool. The tool consists of peripheral cutting edges, a reaming part and a milling part, which have a smaller diameter (d) than that of the peripheral cutting edges (D). The hole made by the milling part has a smaller diameter than required. The reaming part has a nonuniform diameter and connects the milling part to the peripheral cutting edges. The bottom of the reaming part has the same radius as the milling part, and the roof of the reaming part has the same radius as the peripheral cutting edges. The radius of the arc (R) of the ODR tool is larger than the diameter of the tool, and the arc is only tangent to the periphery cutting edge. The reaming part is used to expand the hole made by the milling part. The peripheral cutting edges are of the same form as those on an end mill and can expand the hole to the required diameter. Furthermore, the tool structure is relatively simple to fabricate.

2.2 Hole forming process of ODR

In COD, the axis of an end mill exhibits planetary motion around the axis of the drilled hole while feeding downward; thus, a helical path is formed. The formation of the hole can be decomposed into three stages. (1) The edges on the tool end face reach the workpiece and begin to plunge into the workpiece. (2) When the tool moves along a helical path in the workpiece, the bottom profile of the hole cross section starts

to be shaped like a simple folded line with a drop of $a_p/2$ and retains this shape until the edges on the end face pass through the workpiece [29]. (3) The end face penetrates the workpiece, and the material remaining at the exit of the hole is removed by the peripheral cutting edges of the tool.

Due to the tool geometry, the hole formation process of ODR is more complicated than that of COD. When the workpiece thickness is greater than the height of the reaming part, the hole formation process of ODR can be divided into six stages. Figure 3a–f shows cross sectional drawings of the tool at the crucial height during ODR. (1) The edges on the milling part of the tool touch the workpiece and begin to plunge into the workpiece (Fig. 3a). (2) The tool moves along a helical path in the workpiece. The milling part makes a hole with a diameter of $d + 2e$. The reaming part expands the hole that was made in the previous revolutions by the milling part (Fig. 3b). (3) After the tool has completed n revolutions, the workpiece forms a circumferential groove with its depth reaching h ($n = h/a_p$). Then, at that moment, the reaming part completely immerses into the workpiece. The peripheral cutting edges remove the material that remains on the hole wall. The diameter of the entrance is expanded to $D + 2e$ (Fig. 3c). (4) The tool moves along a helical path in the workpiece, and each part repeats the operation: a hole is made by the milling part, which is expanded by the reaming part and then subsequently expanded to $D + 2e$ by the peripheral cutting edges until the milling part passes through the workpiece and makes a hole with a diameter of d . Delamination often occurs in this stage, and compared with the general end mill, the ODR tool has a smaller milling part and thrust force, which effectively reduces the possibility of delamination (Fig. 3d). (5) In the next revolution, the material remaining at the exit is removed by the reaming part, and the diameter of the exit is expanded to $d_{ap} + 2e$ (Fig. 3e). (6) In the next n revolutions, the reaming part removes the material that remains on the hole wall, and the peripheral cutting edges expand the hole to $D + 2e$ until the milling part passes through the workpiece to a depth of $h + a_p$. The hole exit diameter achieves the required size of $D + 2e$. Thus, the ODR process is completed. In the process of reaming, the milling part does not participate in cutting; the thrust force is kept at a very low level (close to 0) or even a negative value to inhibit the generation and expansion of delamination (Fig. 3f).

It can be seen from the ODR process that the dedicated tool mills a smaller hole at first and expands the diameter of the hole to the required size after multiple reaming processes. Machining with the ODR tool can combine two processes—milling and reaming—into a single process.

3 Experimental setup

3.1 Workpiece material and cutting tool

In this research, the carbon fiber–reinforced composites were composed of carbon fibers and epoxy resin, for which the

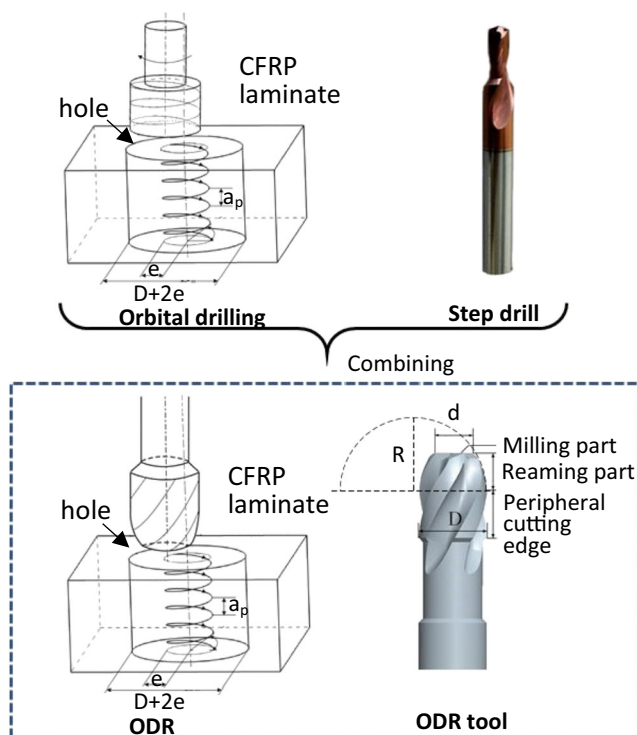
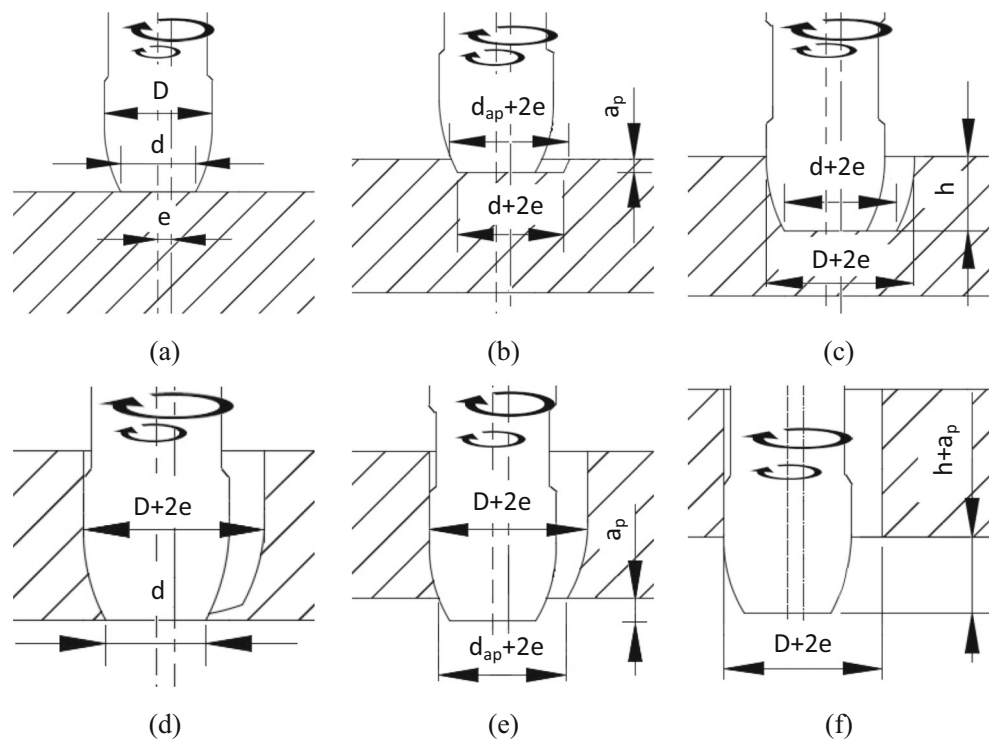


Fig. 2 ODR and the ODR tool

Fig. 3 Hole/tool cross sectional drawings at crucial heights during ODR: **a** contact with the top, **b** expanding the entrance, **c** completion of the entrance, **d** contact with the bottom, **e** expanding the exit, and **f** completion of the exit



volume fractions were 60% and 40%, respectively. The composite was made from 3 k plain unidirectional prepreg (TAIRYFIL TC-33 3 k, polyacrylonitrile (PAN)-based carbon fibers) with epoxy resin as the matrix material. The thickness of each layer was approximately 0.12 mm. The top and the bottom prepreg plies were bidirectional prepreg plies woven by interlacing 0° and 90° fibers, and 36 unidirectional prepreg fiber layers with a symmetrical layout $[0^\circ/+45^\circ/90^\circ/-45^\circ]_{9s}$ were in the middle of the composite. The tensile strength of the composite was 2400 MPa, and the Young's modulus was 160 GPa. The manufacturing process included compression molding, high-temperature curing and cutting, and the CFRP was cut to dimensions of 90 mm \times 90 mm \times 5 mm.

A general end mill and an ODR tool were adopted in the experiment; details of the tools are listed in Table 1.

3.2 Experimental conditions

To compare the machining performance of the two kinds of tools, an empirical study of the thrust force and tool wear was conducted. The first set of tests was based on machining CFRPs with orbital drilling and employed the same experimental conditions while installing different types of tools. The experiments were carried out using a VM7032 CNC milling machine with a spindle speed as high as 8000 rpm. A fixture that ensured drilling without a support backplate was developed and used throughout the experiments. A type 9257B Kistler dynamometer was used to record the forces in the drilling process. The experimental setup is shown in Fig. 4.

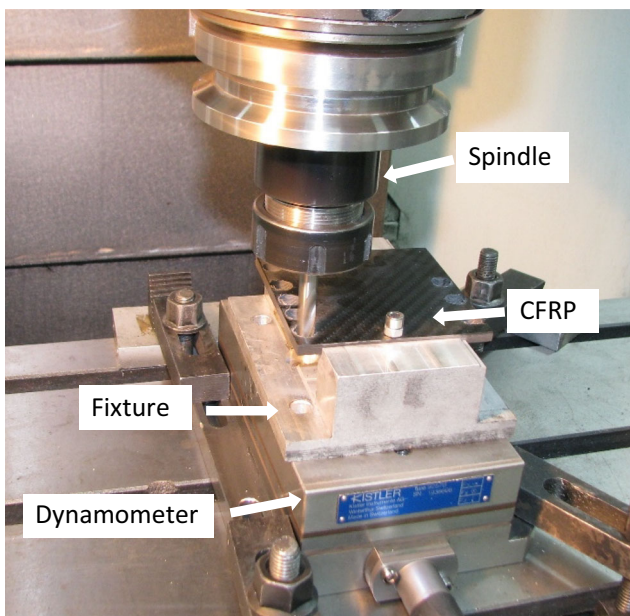
A random experiment was conducted on the cutting force and the wear state of the tools. The machining conditions were a hole diameter of 10 mm (eccentricity of 1 mm), a Z-axis feed rate of $v_{fa} = 0.01$ mm/rev, a tangential feed rate of $v_{ft} = 0.063$ mm/rev, and a tool rotational speed of 1500 rpm (cutting speed of 95.4 mm/min). The cutting force and the flank wear width were measured every 10 holes, and each tool was tested for 160 bores because the tool wear of the general end mill reached the threshold for determining the tool life in accordance with ISO 8688 (maximum flank wear of 0.3 mm).

Variable spindle speeds in the second set of tests helped to achieve cutting temperature comparisons between the two kinds of tools. A VM7032 CNC milling machine and an FLIR A315 thermal infrared imager were used in the test. The experimental facility is shown in Fig. 5a, and an infrared image of the workpiece is shown in Fig. 5b. The thermal infrared imager was placed on one side of the workpiece and focused on the sidewall of the workpiece. Four points were marked in the infrared image: Sp4 showed the background temperature, whereas Sp1-3 showed the temperature at three points at different heights on the sidewall. The holes made in this test were required to be as close together as possible to the sidewall of the workpiece. To ensure the integrity of the hole wall and to truly show the variation in the cutting temperature, the axis of the hole was 6 mm away from the workpiece boundary (the hole radius was 5 mm in this test). This approach can show the effect on the temperature of different tools, although the temperature field distribution was slightly different from that during actual industrial production. Each

Table 1 Details of the cutters

Tool type	Feature	Value
General end mill	Tool diameter	8 mm
	Carbide	K20
	Helix angle	30°
	Coated	No
	Flutes	4
	Rake angle of the end teeth and peripheral cutting edges	7°
	Tool clearance of the end teeth and peripheral cutting edges	7°
ODR tool	Diameter of the milling part	5.5 mm
	Diameter of the peripheral cutting edges	8 mm
	Radius of the arc of the ODR tool	10.625 mm
	Height of the reaming part	5 mm
	Carbide	K20
	Helix angle	30°
	Coated	No
	Flutes	4
	Rake angle of the milling part, reaming part and peripheral cutting edges	7°
Tool clearance of the milling part, reaming part and peripheral cutting edges	7°	

tool was tested for three bores. The use of new tools in each machining instance avoided the effects of tool wear on the experimental results. The machining conditions included a hole diameter of 10 mm (an eccentricity of 1 mm), a Z-axis feed rate of $v_{fa} = 0.01$ mm/rev, and a tangential feed rate of $v_{ft} = 0.063$ mm/rev. To achieve this aim, three different spindle speeds were selected: 1500 rpm (cutting speed of 95.4 mm/min), 2000 rpm (cutting speed of 127.2 mm/min), and 2500 rpm (cutting speed of 159 mm/min). The experiment was repeated three times, and the results were recorded.

**Fig. 4** The experimental setup in test 1

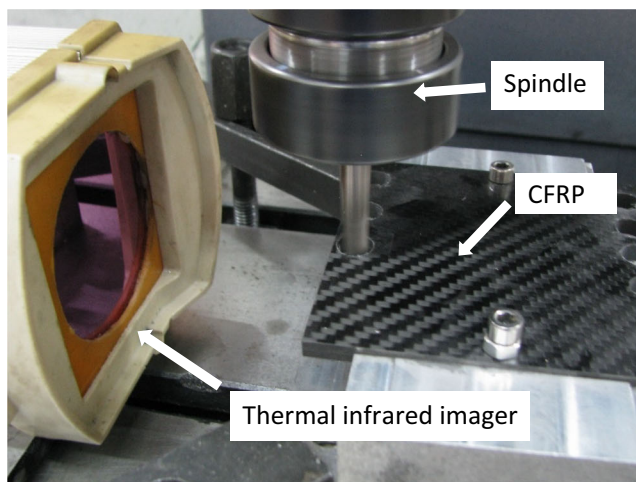
All the experiments adopted dry machining, and a vacuum cleaner was not used. The exit quality and the tool wear were measured using an Anyty 3R-WM401 portable digital microscope.

4 Results and discussion

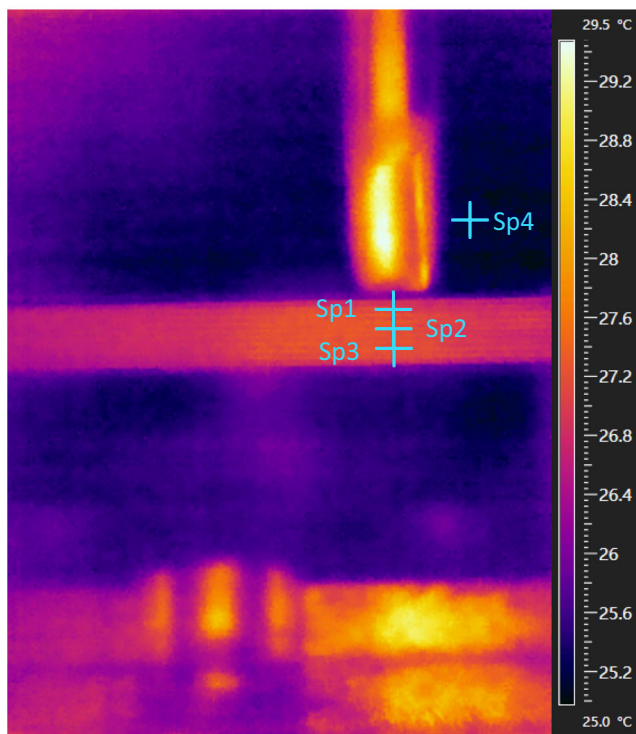
4.1 Thrust forces and tool wear

The ODR process was divided into six stages, as shown in Fig. 3. When the thickness of the workpiece was not greater than the height of the reaming part, stages c, d, and e will merge into two stages. In test one, the workpiece thickness was the same as the reaming part height, and stages c and d took place at the same time. The raw data of the cutting force during ODR are shown in Fig. 6.

Figure 6 shows that the thrust forces reached the maximum value during the machining process in stage a. In stage b, the thrust forces decreased but fluctuated at a specific frequency and amplitude. This was probably due to the thickness reduction in the remaining material, which reduced the thrust force. The leading cause of the thrust force fluctuations was the periodic variation in the layup direction of the CFRP plate. The number of thrust force fluctuations in stage b was approximately equal to the number of cycles in the layup orientation. In stages c and d, the thrust force reached the minimum value of smooth cutting because the milling part was about to pass through the bottom of the material. The milling part was the primary contributor to the thrust force, and the thrust forces approached zero when the milling part passed through the



(a)



(b)

Fig. 5 a Experimental setup in test 2 and b an infrared image of the workpiece

workpiece in stage e. In stage f, the thrust forces maintained a low level (near zero) until the ODR process was completed. In this experiment, the ODR process took approximately 40 s to complete. It can also be observed that the forces in the X and Y directions increased during the entry of the reaming part and decreased with the exit from the workpiece.

The raw data of the cutting force of the COD are shown in Fig. 7. Compared with the trend of the cutting force in the ODR process, the trend of the cutting force in the COD process was much simpler. Figure 7 shows that the thrust forces reached the maximum values in stage 1. In stage 2, the thrust forces gradually decreased but fluctuated at a specific

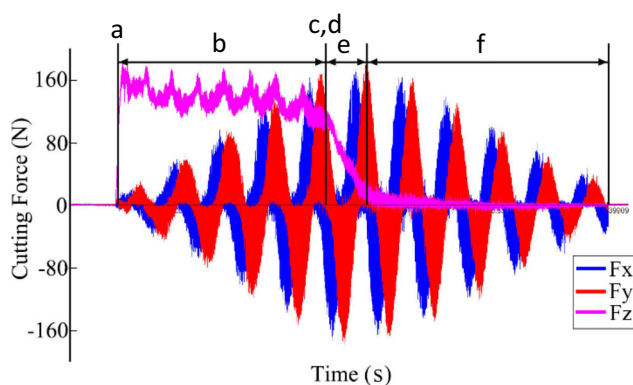


Fig. 6 Cutting force of ODR

frequency and amplitude. In stage 3, the thrust forces approached approximately zero and maintained a low level (near zero) until the COD process was completed. In this experiment, the COD took approximately 20 s to complete. The amplitude of the force fluctuations in the X and Y directions remained unchanged during the process.

The maximum thrust force and tool wear during the COD process and the ODR process in test 1 are shown in Fig. 8. The workpiece was fixed on the fixture and suspended with a large span, and the thrust force was affected by the deformation of the workpiece during machining. Due to the installation of the workpiece and the position of the drilled hole, the axial force of the hole near the fixture was large. The maximum axial force fitting curve is also shown in Fig. 8, wherein the influence of the hole position is considered. The thrust force generated by the ODR tool was approximately 20% less than that of the general end mill, and the thrust force increased on a small slope with an increase in the number of holes. Comparing the thrust forces in the COD process and the ODR process, the most obvious difference was that the thrust forces generated by the ODR tool were much lower than those generated by the general end mill. Moreover, there was a stage in the ODR process in which the reaming part expanded the exit of the hole while maintaining the thrust force at a low level (near zero). Process of reaming is a reliable guarantee of a high-quality exit without delamination.

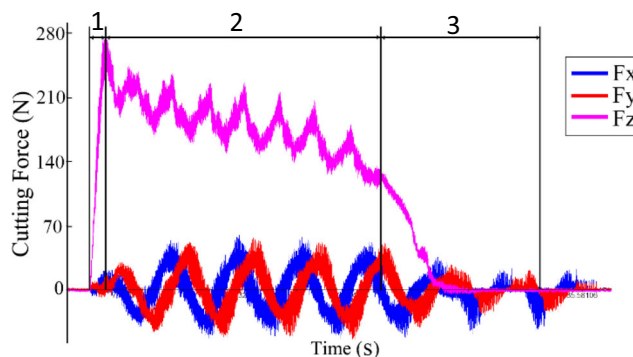
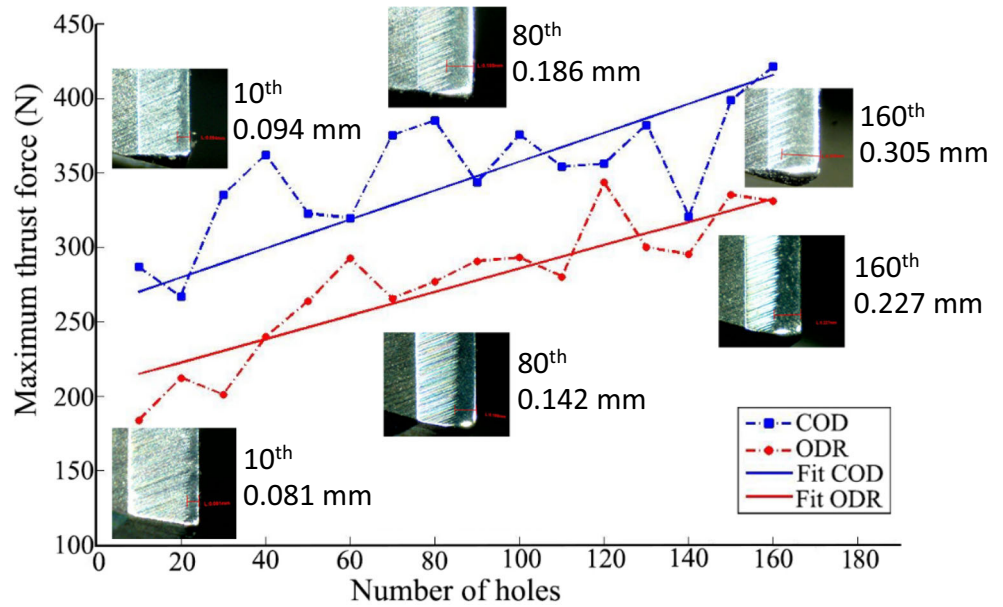


Fig. 7 Cutting force of COD

Fig. 8 Maximum thrust force and tool wear of the ODR tool and general end mill

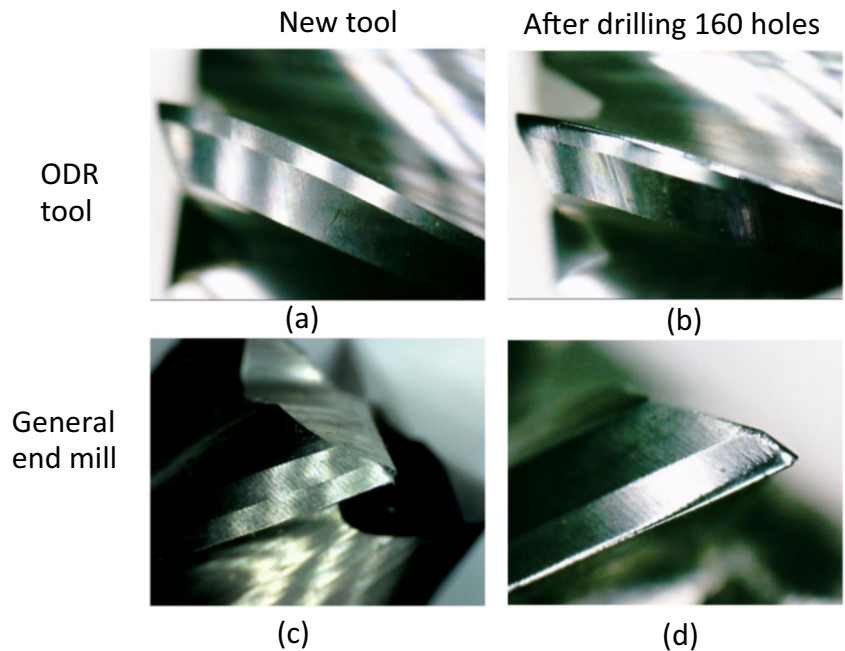


To make the tools wear out quickly, uncoated tools were used in test 1. The tool wear was investigated with a microscope. Figure 8 shows the flank wear of the milling part of the 10th, 80th, and 160th holes. An increase in tool wear and maximum thrust force was noticed as the number of drilled holes increased. The teeth of both new tools were quite sharp in test 1. Figure 8 depicts images of the flank face of a tooth from the ODR tool and general end mill. After drilling 10 holes, the wear rate on the flank face in the *X*-direction was approximately 0.081 mm and 0.094 mm for the ODR tool and general end mill, respectively. After drilling 80 holes, these

wear rates were approximately 0.141 mm and 0.186 mm, respectively; hence, the tooth of the general end mill sustained moderate wear at this point. After drilling 160 holes, the wear rates of the ODR tool and general end mill were 0.227 mm and 0.305 mm, respectively. At this point, severe wear traces were observed on the general end mill, and the ODR tool had sustained moderate wear.

The tool wear on the peripheral cutting edge of the general end mill and the tool wear on the reaming part and the peripheral cutting edges of the ODR tool were also investigated, and the results are shown in Fig. 9.

Fig. 9 Tooth wear conditions on the peripheral cutting edge of two kinds of tools: **a** peripheral cutting edge of a new ODR tool, **b** peripheral cutting edge of the ODR tool after drilling 160 holes, **c** peripheral cutting edge of a new end mill, and **d** peripheral cutting edge of an end mill after drilling 160 holes



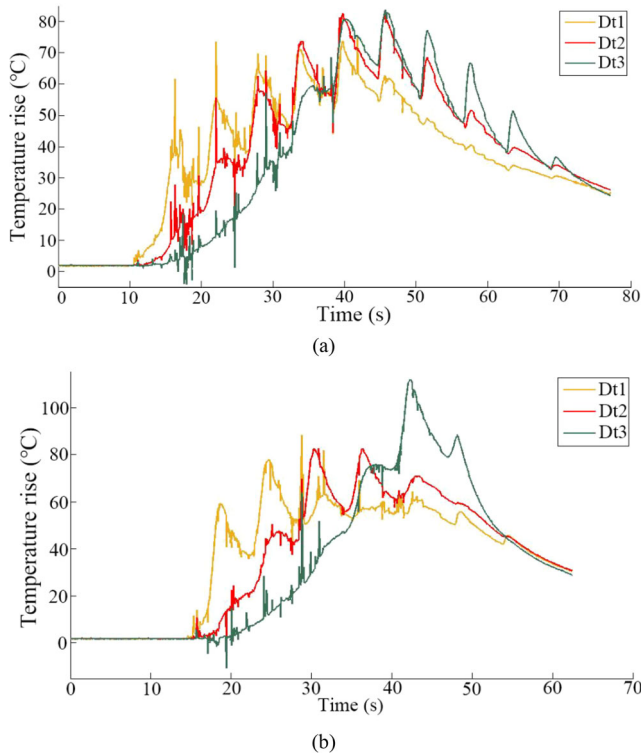


Fig. 10 Temperature rise during **a** ODR and **b** COD (eccentricity = 1 mm, $v_{fa} = 0.01$ mm/rev, $v_{fi} = 0.063$ mm/rev, and spindle speed = 2500 rpm)

The junction between the reaming part and the peripheral cutting edges of the ODR tool is shown in Fig. 9 a and b. The peripheral edge of the general end mill is shown in Fig. 9 c and d. Figure 9b shows that the reaming part of the ODR tool was fully utilized, and mild wear can be observed on the whole reaming part. As shown in Fig. 9d, only a small part of the peripheral edge close to the end face was worn out. Affected by the principle of COD, only a small part of the peripheral edge was involved in machining, and this part was close to the end face. The lack of utilizing most parts of the peripheral cutting edges shortens the tool life, thereby resulting in a large amount of waste and increases in cost.

4.2 Cutting temperatures

To investigate the impact of different cutting tools on temperature, a FLIR A315 thermal infrared imager was used to measure the temperature on the hole wall. The temperature rise on the hole wall during the ODR process, and the COD process was obtained from the thermal infrared images, and the results

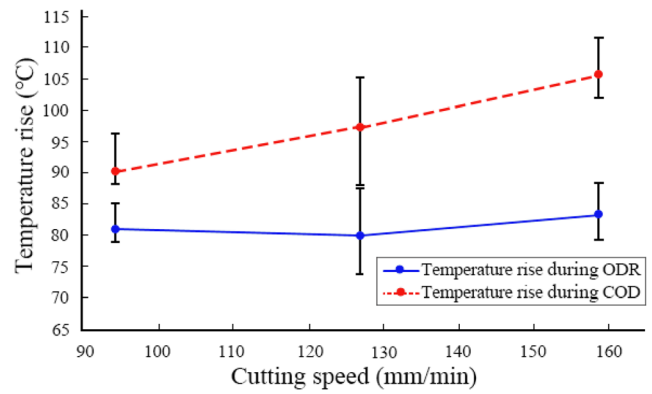


Fig. 11 Impact of the cutting speed and cutting tools on the temperature rise during machining

are shown in Fig. 10 and Table 2. Dt1, Dt2, and Dt3 indicate the temperature rise between the marked points Sp1, Sp2, and Sp3 and the ambient temperature Sp4. Sp1 was 1 mm away from the upper layer of the workpiece, Sp3 was 1 mm away from the bottom of the workpiece, and Sp2 was 1.5 mm away from Sp1.

Figure 10 shows that the maximum temperature rise during COD was greater than that during ODR. Each fluctuation in the curves shown in this figure represents the completion of a processing revolution of the tool, which travels closer to and then farther away from the measuring point. Affected by the tool shape, the temperature rise during a single processing revolution is limited, the number of processing revolutions at each marked point is very high, and the heat dissipation during the process is more efficient. Heat accumulation is the main cause of the temperature rise during ODR. In the observation of the temperature rise of Sp1, Sp2, and Sp3, it can be found that when the temperature of one marked point changes, the measuring point that lies above it also changes with the same trend but a small amplitude. This finding indicates that the heat source is distributed in the Z-direction. In contrast to the ODR, during COD, there is a slight interaction between the marked points, and the temperature changes at each marked point are relatively independent, which indicates that the heat source is relatively concentrated in the Z-direction. Moreover, the number of processing revolutions at each marked point is relatively low, but the temperature rise during each single processing revolution is very high. The heat accumulation and the large temperature rise during a single processing revolution work together, resulting in a higher maximum temperature rise in the COD.

Table 2 Exit delamination factor of different cutting tools

	1st hole	40th hole	80th hole	120th hole	160th hole
ODR tool	1	1	1.13	1.15	1.14
General end mill	1.11	1.32	1.23	1.38	1.41

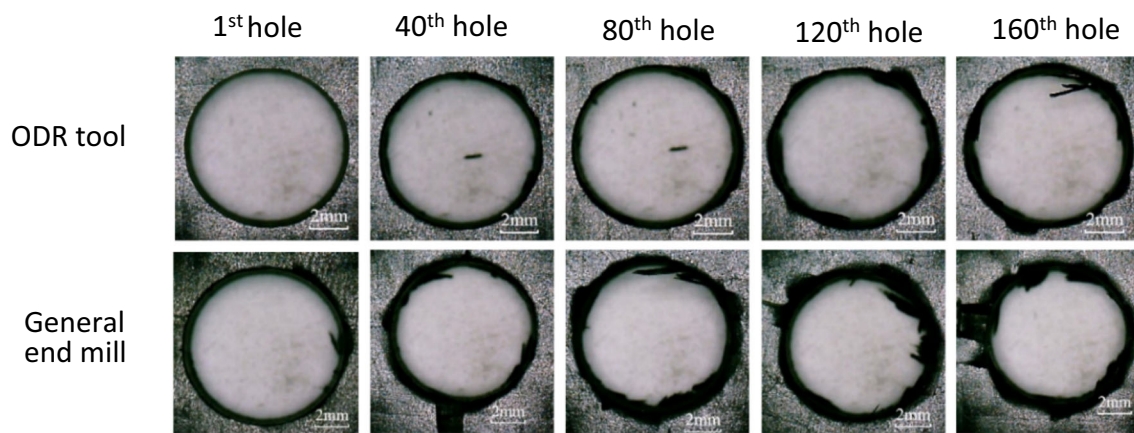


Fig. 12 Burrs on the exits of holes drilled by two kinds of tools

The maximum temperature rise in the two kinds of tools is shown in Fig. 11. As presented, compared with the general end mill, the ODR tool has a lower processing temperature. Especially in high-speed machining, the discrepancy in the temperature rise between the two kinds of tools is more prominent.

4.3 Burrs and delamination

An optical microscope was used to observe the delamination and burrs. The burrs on the hole exits obtained by the ODR tool and the general end mill were observed, and the results are shown in Fig. 12.

Manufacturing holes with the ODR tool can reduce the degree of damage compared with manufacturing holes with the general end mill. Even more importantly, note that the cutting action of the reaming part eradicates the burrs caused by the milling part, as shown in Fig. 13.

Figure 13a shows that on the exit, there is quite a large burr, which was cut into small pieces during the next revolution (as shown in Fig. 13b) and is nearly entirely removed after several cutting revolutions (as shown in Fig. 13c).

When attempting to reduce defects, much attention is focused on delamination—including peel-up delamination at the entrances of holes and push-down delamination at the exits of holes—and burr formation; however, the primary focus is on delamination. The occurrence of delamination damage cannot be completely avoided with the application of two kinds of tools. Delamination was also observed at the exits of holes during the ODR process and the COD process in Fig. 12. Many push-down delaminations and severe damage can be observed at the hole exit in the COD. However, the ODR process did not cause severe damage at the hole exit. For an intuitive comparison, the delamination levels of the holes were quantified. The delamination factor is calculated for different tools with Eq. 1. The factor, expressed as F_d , is the ratio of the maximum diameter in the damaged zone (expressed as D_{\max}) to the hole diameter, which is expressed as D_{nom} [35].

$$F_d = \frac{D_{\max}}{D_{\text{nom}}} \quad (1)$$

Table 2 shows the impact of the number of holes machined on the delamination factor (F_d) of different cutting tools.

The degree of tool wear increased as the number of machined holes increased, and the processing quality of the general end

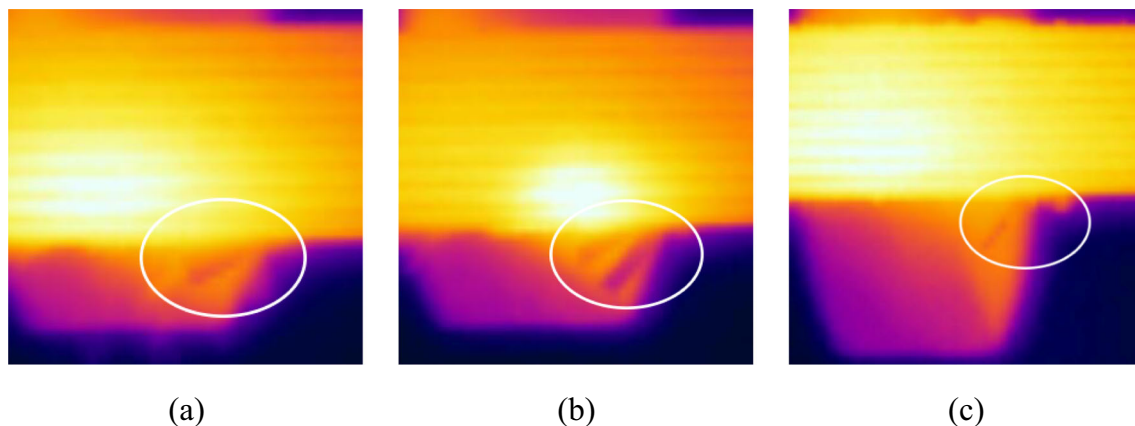


Fig. 13 Burrs removed by reaming part: **a** a burr appears, **b** the burr is cut up, and **c** most of the burr has been removed

mill gradually deteriorated. However, the ODR tool has always demonstrated good processing quality. Even if the tool was moderately worn, the machining quality was not seriously affected.

The primary goal of industrial applications is to minimize delamination for optimal use of tools and to extend tool life. Machining with ODR is indeed a better approach than machining with COD, even though the former takes slightly longer than the latter. The ODR process provides a minor delamination factor, less thrust force, lower cutting temperature, and longer tool life, which has good prospects towards industrial application.

Under the same cutting conditions, the machining performance of two kinds of tools were studied in this paper, such as cutting force, tool life, cutting temperature, and machining quality. Nevertheless, how to further improve the machining performance of ODR tool has not been studied in this paper. Therefore, this will be the main direction of future work. The authors intend to study the influence of input parameters on machining performance and optimize the operation time with a method of variable feed rate to shorten the time of exit expansion.

5 Conclusion

In this research, the author proposed a dedicated tool for orbital drilling of CFRPs. The ODR tool, which contains a milling part, a reaming part and peripheral cutting edges, is more complex than a general end mill. With the help of this novel tool, COD can be improved to a process of ODR, which combines two processes—milling and reaming—into one process. The ODR tool was analyzed geometrically, and experiments were carried out to verify the machining performance of ODR tool for CFRPs; the processing results from the ODR tool were compared with though from the general end mill.

1. Compared with the general end mill, the ODR tool reduces the thrust force and improves the processing quality by reducing burrs and delamination. The cutting temperature of the ODR tool is also significantly lower than that of the COD tool, and this discrepancy is more obvious under a higher cutting speed.
2. Under the same processing conditions, the tool life of the ODR tool is significantly higher than that of the general end mill, and the ODR tool can create more holes with higher processing quality.
3. The ODR tool is easy to popularize and apply in industry because it offers quality improvements without increasing costs. The ODR tool is relatively easy to fabricate, and the ODR process can be executed with the same equipment as the COD process.

Funding information This work was supported by the National Key Research and Development Program of China under Grant No. 2019YFB1704803.

References

1. Bonnet C, Poulachon G, Rech J, Girard Y, Costes J (2015) CFRP drilling: fundamental study of local feed force and consequences on hole exit damage. *Int J Mach Tools Manuf* 94:57–64
2. Shyha I, Aspinwall D, Soo S, Bradley S (2009) Drill geometry and operating effects when cutting small diameter holes in CFRP. *Int J Mach Tools Manuf* 49(12-13):1008–1014
3. Gao Y, Xiong J, Xiao J, Lu D (2019) A tilted orbital grinding technique for hole-making of CFRP composite laminates. *Int J Adv Manuf Tech* 104(1-4):661–673
4. Faraz A, Biermann D, Weinert K (2009) Cutting edge rounding: an innovative tool wear criterion in drilling CFRP composite laminates. *Int J Mach Tools Manuf* 49(15):1185–1196
5. Abrão A, Faria P, Rubio J, Reis P, Davim J (2007) Drilling of fiber reinforced plastics: a review. *J Mater Process Tech* 186(1-3):1–7
6. Srinivasan T, Palanikumar K, Rajagopal K, Latha B (2016) Optimization of delamination factor in drilling GFR–polypropylene composites. *Mater Manuf Process* 32(2):226–233
7. Durão L, Gonçalves D, Tavares J, Albuquerque V, Vieira A, Marques A (2010) Drilling tool geometry evaluation for reinforced composite laminates. *Compos Struct* 92(7):1545–1550
8. Iliescu D, Gehin D, Gutierrez M, Girof F (2010) Modeling and tool wear in drilling of CFRP. *Int J Mach Tools Manuf* 50(2):204–213
9. Tsao C, Hocheng H (2003) The effect of chisel length and associated pilot hole on delamination when drilling composite materials. *Int J Mach Tools Manuf* 43(11):1087–1092
10. Jain S, Yang D (1994) Delamination-free drilling of composite laminates. *J Eng Indus* 116(4):475–481
11. Qiu X, Li P, Niu Q, Chen A, Ouyang P, Li C, Ko T (2018) Influence of machining parameters and tool structure on cutting force and hole wall damage in drilling CFRP with stepped drills. *Int J Adv Manuf Tech* 97(1-4):857–865
12. Isbilir O, Ghassemieh E (2013) Numerical investigation of the effects of drill geometry on drilling induced delamination of carbon fiber reinforced composites. *Compos Struct* 105:126–133
13. Feito N, Díaz-Álvarez J, López-Puente J, Miguelez M (2018) Experimental and numerical analysis of step drill bit performance when drilling woven CFRPs. *Compos Struct* 184:1147–1155
14. Lazar M, Xirouchakis P (2011) Experimental analysis of drilling fiber reinforced composites. *Int J Mach Tools Manuf* 51(12):937–946
15. Hocheng H, Tsao C (2005) The path towards delamination free drilling of composite materials. *J Mater Process Tech* 167(2-3): 251–264
16. Biermann D, Bathe T, Rautert C (2017) Core drilling of fiber reinforced materials using abrasive tools. *Procedia CIRP* 66:175–180
17. Su F, Zheng L, Sun F, Wang Z, Deng Z, Qiu X (2018) Novel drill bit based on the step-control scheme for reducing the CFRP delamination. *J Mater Process Tech* 262:157–167
18. Jia Z, Fu R, Niu B, Qian B, Bai Y, Wang F (2016) Novel drill structure for damage reduction in drilling CFRP composites. *Int J Mach Tools Manuf* 110:55–65
19. Butler-Smith P, Axinte D, Daine M, Kennedy A, Harper L, Bucourt J, Ragueneau R (2015) A study of an improved cutting mechanism of composite materials using novel design of diamond micro-core drills. *Int J Mach Tools Manuf* 88:175–183
20. Tsao C (2008) Investigation into the effects of drilling parameters on delamination by various step-core drills. *J Mater Process Tech* 206(1-3):405–411
21. Geier N, Davim J, Szalay T (2019) Advanced cutting tools and technologies for drilling carbon fibre reinforced polymer (CFRP) composites: a review. *Composites Part A: Applied Science and Manufacturing*, 105552

22. Pereszlai C, Geier N (2020) Comparative analysis of wobble milling, helical milling and conventional drilling of CFRPs. *Int J Adv Manuf Tech* 106(9-10):3913–3930
23. Xu W, Zhang L (2014) On the mechanics and material removal mechanisms of vibration-assisted cutting of unidirectional fibre-reinforced polymer composites. *Int J Mach Tools Manuf* 80:1–10
24. Alberdi A, Suárez A, Artaza T, Escobar-Palafox G, Ridgway K (2013) Composite cutting with abrasive water jet. *Prod Eng* 63:421–429
25. Herzog D, Jaeschke P, Meier O, Haferkamp H (2008) Investigations on the thermal effect caused by laser cutting with respect to static strength of CFRP. *Int J Mach Tools Manuf* 48(12-13):1464–1473
26. Teicher U, Müller S, Münzner J, Nestler A (2013) Micro-EDM of carbon fibre-reinforced plastics. *Procedia CIRP* 6:320–325
27. Pereira R, Brandão L, Paivab A, Ferreira J, Davim J (2017) A review of helical milling process. *Int J Mach Tools Manuf* 120:27–48
28. Brinksmeier E, Fangmann S, Meyer I (2008) Orbital drilling kinematics. *Prod Eng* 2(3):277–283
29. Tanaka H, Kitamura M, Sai T (2015) An evaluation of cutting edge and machinability of inclined planetary motion milling for difficult-to-cut materials. *Procedia CIRP* 35:96–100
30. Voss R, Henerichs M, Kuster F (2016) Comparison of conventional drilling and orbital drilling in machining carbon fibre reinforced plastics (CFRP). *CIRP Ann* 65(1):137–140
31. Ahmad N, Khan S, Raza S (2019) Influence of hole diameter, workpiece thickness, and tool surface condition on machinability of CFRP composites in orbital drilling: a case of workpiece rotation. *Int J Adv Manuf Tech* 103(5-8):2007–2015
32. Zhou L, Ke Y, Dong H, Chen Z, Gao K (2016) Hole diameter variation and roundness in dry orbital drilling of CFRP/Ti stacks. *Int J Adv Manuf Tech* 87(1-4):811–824
33. Ohta K, Tanaka H, Takizawa R (2012) Development of tilted planetary drilling system. *Procedia CIRP* 1:681–682
34. Wang Q, Wu Y, Bitou T, Nomura M, Fujii T (2018) Proposal of a tilted helical milling technique for high quality hole drilling of CFRP: kinetic analysis of hole formation and material removal. *Int J Adv Manuf Tech* 94(9-12):4221–4235
35. Chen W (1997) Some experimental investigations in the drilling of carbon fiber-reinforced plastic (CFRP) composite laminates. *Int J Mach Tools Manuf* 37(8):1097–1108

Publisher's note Springer Nature remains neutral with regard to jurisdictional claims in published maps and institutional affiliations.